J Soils Sediments (2010) 10:870–878
DOI 10.1007/s11368-010-0219-1

ISMESS 2009 • RESEARCH ARTICLE

Pb^{2+} adsorption on birnessite affected by Zn^{2+} and Mn^{2+} pretreatments

Wei Zhao · Qing Qing Wang · Fan Liu · Guo Hong Qiu · Wen Feng Tan · Xiong Han Feng

Received: 30 October 2009 / Accepted: 8 March 2010 / Published online: 9 April 2010

Abstract
Purpose Lead contamination is ubiquitous, and much attention has been paid due to its toxicity. The phyllomanganate birnessite is the most common Mn oxide in soils. The MnO_6 octahedral layers may have significant Mn vacancies in the hexagonal birnessites. Among heavy metal ions, birnessites possess the greatest adsorption affinity and capacity for Pb^{2+}. The aim of this study was to understand the relationship between vacant Mn octahedral sites and Pb^{2+} adsorption.
Materials and methods Birnessite synthesis was achieved by the reduction of potassium permanganate in a strong acidic medium. Synthetic birnessite was then treated with Mn^{2+} or Zn^{2+} at different concentrations. Isothermal Pb^{2+} adsorption on birnessite before and after treatments was measured at a solid-to-liquid ratio of approximately 1.67 g/L, and Pb^{2+} concentrations ranged from 0 to 10 mmol/L with an ionic strength of 0.1 mol/L $NaNO_3$. The amount of Pb^{2+} adsorbed and the amount of Mn^{2+} or Zn^{2+} released during the whole adsorption process were obtained by comparison with a control group without adding Pb^{2+}. The amount of H^+ released was determined from the recorded additions of standard HNO_3/NaOH solutions.
Results and discussion Mn average oxidation state (AOS) and d(110)-interplanar spacings of the birnessites remained almost unchanged as the concentration of the treating Zn^{2+} increased, indicating an unchanged number of vacant Mn octahedral sites, whereas the maximum Pb^{2+} adsorption decreased from 3,190 to 2,030 mmol/kg due to the presence of Zn^{2+} on adsorption sites. The AOS's of the Mn^{2+}-treated birnessites decreased and most of the Mn^{2+} ions added were oxidized to Mn^{3+} ions. The d(110)-interplanar spacing of Mn^{2+}-treated birnessites increased from 0.14160 to 0.14196 nm, indicative of a decreased vacant Mn octahedral sites. Moreover, the maximum Pb^{2+} adsorption of Mn^{2+}-treated birnessites decreased from 3,190 to 1,332 mmol/kg, the decrease being greater than that for the corresponding Zn^{2+}-treated birnessites.
Conclusions Most Mn^{2+} was oxidized to Mn^{3+} by birnessite, with a portion of Mn^{3+} located above or below vacant sites, which did not affect the number of vacant sites, and the remaining Mn^{3+} migrating to occupy the vacant sites. In contrast, Zn^{2+} ions are adsorbed only above or below vacant sites. Birnessite Pb^{2+} adsorption capacity is determined largely by the number of vacant Mn sites.

Keywords Birnessite · Pb^{2+} adsorption · Vacant Mn octahedral sites · Zn^{2+} adsorption

Responsible editor: Caixian Tang

W. Zhao · Q. Q. Wang · F. Liu (✉) · G. H. Qiu · W. F. Tan · X. H. Feng
Key Laboratory of Subtropical Agriculture Resource and Environment, Ministry of Agriculture,
Huazhong Agricultural University,
Wuhan 430070, People's Republic of China
e-mail: liufan@mail.hzau.edu.cn

W. Zhao
State Key Laboratory of Soil Erosion and Dryland Farming on Loess Plateau, Institute of Soil and Water Conservation,
Chinese Academy of Sciences and Ministry of Water Resources,
No.26, Xinong Road,
Yangling, Shaanxi 712100, People's Republic of China

1 Introduction

Lead is an environmental heavy metal that has always attracted much attention. Adsorption is one of the important processes that affect the transfer of heavy metals including Pb from the aqueous to solid phase and, thus, influence

their distribution, mobility, and bioavailability (Xu et al. 2006). Manganese (Mn) oxides are widely distributed in soils, sediments, and ocean manganese nodules. They are characterized by low points of zero charge, large surface areas and great amounts of negative charges, and are actively involved in various chemical reactions. They are considered as important Pb adsorbents in the environments (McKenzie 1980; O'Reilly and Hochella 2003; Post 1999). Understanding the reactivity of Mn oxides with Pb is essential to predict the fate and transport of Pb in the environments and to optimize remediation measures (Matocha et al. 2001).

The basic building block of Mn oxides is the MnO_6 octahedron. These octahedra can be joined together by sharing corners or edges into layer structures (or phyllomanganates) (Webb et al. 2005). The phyllomanganate birnessite $(H_a(K^+)_bH_2O_cMn_{tc}{}^{2+,3+}[(Mn_d{}^{3+}, Mn_e{}^{4+}), \Upsilon_f]O_2$, where interlayer species are written to the left of the square brackets and tc refers to interlayer Mn in triple corner-sharing positions above or below vacant Mn octahedral sites (Υ) in the layer (enclosed in square brackets, except for the O atoms), is the most common Mn oxide in soils (Ahn et al. 2006; Chang Chien et al. 2009). The MnO_6 octahedral layers may have significant Mn vacancies, with up to one site out of every six Mn octahedra in the hexagonal birnessites. The interlayer water molecules and cations that compensate the charges created by defects in the Mn octahedral layers have a profound influence on the resulting structure (Webb et al. 2005). Many Mn oxides can be synthesized by direct or indirect transformation of birnessite (Golden et al. 1987; Tu et al. 1994). Birnessite synthesis can be achieved by the reduction of potassium permanganate in a strong acidic medium (McKenzie 1971), which is termed "acid-birnessite" (Villalobos et al. 2003). The resulting birnessite has hexagonal layer symmetry with layers comprising edge-sharing $Mn(IV)O_6$ octahedra, $Mn(III)O_6$ octahedra, and vacant Mn octahedral sites (Villalobos et al. 2006). Some Mn^{2+} and Mn^{3+} ions are located above or below vacant Mn octahedral sites in birnessites (Webb et al. 2005). Studies have indicated that birnessite structural vacancies account for the negative layer charges and are associated with adsorption of Pb, Zn, Cu, Cd, and Ni, oxidation of Co^{2+} and Cr^{3+}, and conversion of birnessite (Appelo and Postma 1999; Burns 1976; Lanson et al. 2002a; Manceau and Charlet 1992; Manceau et al. 2002; Peacock and Sherman 2007; Toner et al. 2006). Feng et al. (2007) found that the adsorption affinity and capacity of birnessites differed for different heavy metal ions. Among heavy metal ions, birnessites possess the greatest adsorption affinity and capacity for Pb^{2+}. Lanson et al. (2002b) and Manceau et al. (2002) noted that around 75% of surface-adsorbed Pb ions on birnessite were located either above or below the vacant Mn sites and shared three-layer oxygen atoms with three-layer Mn atoms, thereby forming a tridentate corner-sharing (TC) interlayer complexes, as determined by extend X-ray absorption fine structure (EXAFS), electron diffraction (ED), and X-ray diffraction (XRD) analyses. The rest of the adsorbed Pb ions were located above or below the empty tridentate cavities, sharing three edges with neighboring MnO_6 in the layer, thereby forming a tridentate edge-sharing (TE) interlayer complexes, as in quenselite. Villalobos et al. (2005) found that a portion of Pb ions formed double-corner-sharing complexes at particle edges of birnessite. Matocha et al. (2001) showed that dissolved Mn^{2+} ions, which were released from birnessite during Pb adsorption, originated from Mn^{2+} or Mn^{3+} ions located above or below vacant cation sites. Manceau et al. (2002) showed that Zn ions adsorbed on birnessite were tetrahedrally or octahedrally coordinated and located either above or below vacant Mn sites. As Zn^{2+} (the radius of Zn^{2+} is 0.074 nm; Pauling 1960) is too large to migrate into vacant sites, vacant Mn octahedral sites will remain unchanged during the adsorption of Zn^{2+} on birnessite.

By using X-ray absorption spectroscopy, Manceau et al. (1997) noted that Co^{2+} was oxidized to Co^{3+} on buserite which collapses to birnessite during dehydration and that Co^{3+} migrated into vacant sites, leading to a decrease in the number of vacant Mn structural sites. Mn^{2+} can be oxidized to Mn^{3+} by birnessite (Tu et al. 1994), and the radius of Mn^{3+} (0.066 nm) is close to that of Co^{3+} (0.063 nm; Pauling 1960), suggesting that the oxidation of Mn^{2+} to Mn^{3+} on birnessite is similar to that of Co^{2+} oxidation to Co^{3+} on buserite, leading to a decrease in vacant Mn sites in birnessite.

Though our previous experimental data have indicated that the Pb^{2+} adsorption capacity of birnessite is related to the number of vacant Mn sites, it is necessary to determine whether the Pb^{2+} adsorption capacity of birnessite is controlled by the number of vacant Mn sites. The aims of this study were to investigate the variances of the birnessite structure, Pb^{2+} adsorption capacity, and Mn^{2+} and Zn^{2+} release before and after Zn^{2+} and Mn^{2+} pre-adsorption treatments, respectively, and thereby to understand the relationship between vacant Mn octahedral sites and Pb^{2+} adsorption and provide some basic data for optimizing remediation measures of lead contaminated soils.

2 Materials and methods

2.1 Preparation of birnessite

Birnessite was synthesized in an acidic medium according to the method described by McKenzie (1971). Synthetic birnessite, designated HB0, was prepared using a 165-mL aliquot of 8 mol/L HCl added dropwise at 0.7 mL/min to a 0.6 mol boiling $KMnO_4$ solution in 900–1,200 mL of

distilled deionized and stirred vigorously during reaction. After further boiling for 30 min, the product was aged for 12 h at 60°C (Feng et al. 2007).

2.2 Treatments of birnessite

Samples (5.0 g) of HB0 were added, respectively, to 3 L aliquots of 1.0, 1.5, 1.8, 2.0, 2.2, and 2.4 mmol/L Mn $(NO_3)_2$ with pH adjusted to 5.0. The reaction was continued for 24 h with vigorous stirring. The pH of the reaction system was maintained at 5.0 by the addition of 0.1 mol/L HNO_3 or 0.1 mol/L NaOH. The samples obtained were designated as Mn1, Mn2, Mn3, Mn4, Mn5, and Mn6, respectively. Treatment of birnessite with Zn^{2+} was similar to that for Mn^{2+}, with concentrations of 1.0, 1.5, 1.8, 2.0, and 2.4 mmol/L Zn used. These samples were designated as Zn1, Zn2, Zn3, Zn4, and Zn6, respectively.

All samples were purified by electrical dialysis at a voltage of 150–220 V until the supernatant conductivity was <20 μS/cm and then dried at 40°C.

2.3 Characterization

XRD analyses were performed using a D/Max-3B diffractometer (Rigaku, Japan) with monochromatic Fe Kα radiation. The diffractometer was operated at a tube voltage of 40 kV and a current of 20 mA. Intensities were measured at $2\theta = 10°–90°$ using a count time of 0.2 s/step. For detailed analyses, rutile was used as an internal standard and intensities were measured at $2\theta = 83°–89°$ using a count time of 7 s/step. Step intervals were 0.02°. Transmission electron microscopic (TEM) analyses were carried out using a CM 12 (Philips, the Netherlands) transmission electron microscope operated at 120 kV. The samples were gently crushed into powder, dispersed in absolute ethyl alcohol, and ultrasonically dispersed prior to deposition on holey carbon films. Specific surface area (SSA) was measured by the method of N_2 adsorption (Quantachrome Autosorb-1, USA). The Mn average oxidation state (AOS) was measured using the oxalic acid–permanganate back-titration method (Kijima et al. 2001).

2.4 Adsorption experiments

Lead, Pb^{2+}, adsorption isotherms of all samples, including HB0, Mn (1–6), and Zn (1–6), was measured using 5-g/L sample suspensions at pH 5.00 using a series of Pb^{2+} solutions at concentrations from 0 to 15 mmol Pb per liter with an ionic strength of 0.15 mol/L $NaNO_3$. The pH of the 5 g/L birnessite suspension was maintained at 5.00 by the addition of 0.1 mol/L HNO_3 or 0.1 mol/L NaOH until the pH value was stabilized to pH 5.00±0.05. Then, a 5 mL aliquot of the birnessite suspension was mixed with 10 mL of Pb^{2+} solutions with a range of initial concentrations in 50-mL polyethylene centrifuge tubes. A solid-to-liquid ratio of approximately 1.67 g/L was obtained and the Pb^{2+} concentrations ranged from 0 to 10 mmol/L with an ionic strength of 0.1 mol/L $NaNO_3$ during the reaction. The vials were then capped and shaken for 24 h at 25±1°C. The pH of the reaction system was maintained at 5.00±0.05 by hourly addition of NaOH or HNO_3 using a pH-stat technique with amounts of 0.1 mol/L HNO_3/NaOH solution. Finally, the vials were centrifuged at 14,000 rpm for 10 min and the supernatants collected and analyzed for Pb^{2+} and Mn^{2+} or Zn^{2+} using a Varian AAS 240FS atomic absorption spectrometer (Varian, Australia). The amount of Pb^{2+} adsorbed and the amount of Mn^{2+} or Zn^{2+} released during the adsorption process were obtained by comparison with a control group without added Pb^{2+}. The amount of H^+ released was determined from the recorded additions of standard HNO_3/NaOH solutions. All measurements were performed in triplicate and averaged.

Calculation of chemical equilibrium ensured that no $PbCO_3$ precipitates were formed under the above conditions during the Pb^{2+} adsorption experiment.

3 Results

3.1 Characterization

Powder XRD patterns indicate that the Mn series samples had four characteristic peaks at 0.729, 0.364, 0.245, and 0.141 nm (Fig. 1a), and the Zn series samples had three characteristic peaks at 0.727, 0.357, and 0.244 nm (see Fig. 1b). These primary peaks are characteristic of birnessite without any impurities. Therefore, the structure remained unchanged before and after treatment, though there are some minor differences in the shape and positions of some peaks. It is not clear why the diffraction peaks broadened after treatment with Zn^{2+} (see Fig. 1b).

The range in concentration of Mn^{2+} added in the Mn series, from 1.0 to 2.4 mmol/L, was identical to that for Zn^{2+} in the Zn series. When the concentration of Mn^{2+} in the Mn series equalled that of Zn^{2+} in the Zn series, the adsorption of Mn^{2+} on HB0, from 560 to 1,440 mmol/kg, was similar to that for Zn^{2+} adsorbed on HB0, from 600 to 1,410 mmol/kg (Table 1).

The AOSs of the Mn series samples decreased from 3.96 to 3.75 with added Mn^{2+}, and their SSA ranged from 27.6–67.0 m^2/g. In comparison, the AOSs of the Zn series samples ranged from 3.94 to 3.96, but were almost unchanged as addition of Zn^{2+} increased, and their SSAs ranged from 37.2 to 63.6 m^2/g. The SSAs of the Mn and Zn series samples were larger than that of the HB0 (9.84 m^2/g, Table 2).

The morphology and particle sizes of Mn- and Zn-treated samples and for HB0 were similar (Fig. 2). They

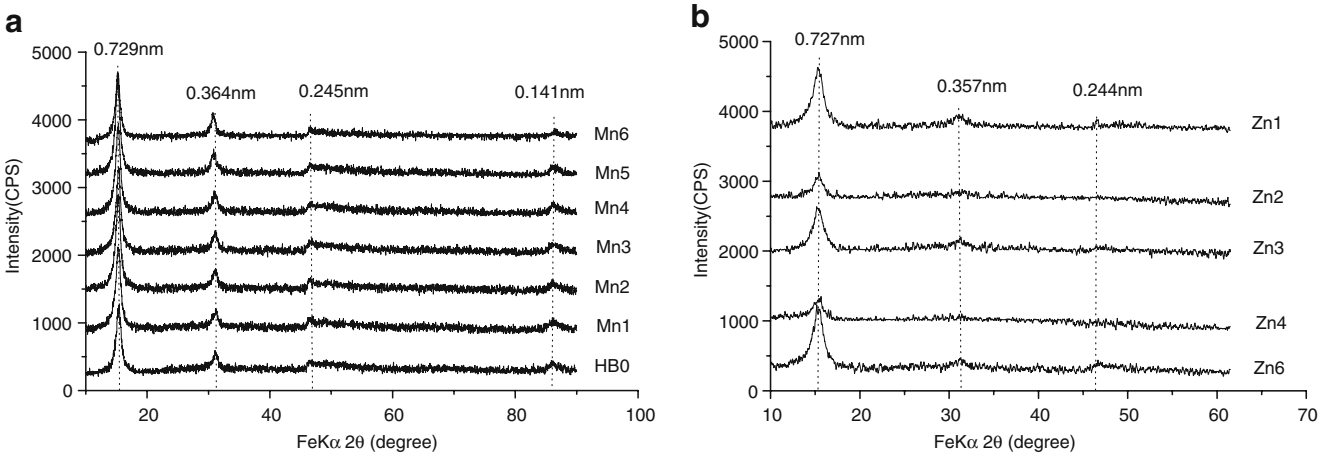

Fig. 1 Powder XRD patterns of all samples. The rutile was not added in this case. **a** Mn series. **b** Zn series

consist of clusters of 100- to 200-nm spherical aggregates which are consistent with the balls of needles described by McKenzie (1971). The balls are actually randomly stacked aggregates of thin plates (Feng et al. 2007).

Diffraction peaks of the (110) crystal plane for all birnessite samples were obtained using two-peak Gaussian fitting of diffraction patterns over the range 84–89° 2θ, which were calibrated using the (310) diffraction peak of rutile (Fig. 3). The high-angle shoulder on the birnessite 110 peak is the (113) reflection for birnessite (see Fig. 3). The (110) interlayer spacing for the HB0 sample is 0.14160 nm. The (110) interlayer spacing for the Mn series birnessites increased from 0.14160 (ie HB0) to 0.14196 nm as the Mn^{2+} concentration increased from 1.0 to 2.4 mmol/L. However, the (110) interlayer spacing for the Zn series birnessites remained almost constant compared to HB0 as the concentration of Zn^{2+} increased.

3.2 Isothermal adsorption

The similarly shaped Pb^{2+} adsorption isotherms (Fig. 4) for all samples are described as L-type isotherms (Giles et al. 1960). All the adsorption isotherms were fitted using the following Langmuir nonlinear model, and the resulting fitting parameters are listed in Table 3.

$$Y = A_{max}KC/(1+KC)$$

where Y is the amount adsorbed per unit weight (mmol/kg), A_{max} represents the maximum Pb^{2+} adsorption, C is the equilibrium Pb^{2+} concentration, and K is a constant related to adsorption energy as a function of adsorption enthalpy and temperature (Kinniburgh 1986).

The maximum Pb^{2+} adsorption decreased from 3,190 to 1,332 mmol/kg (see Table 3), and AOS values of the Mn series birnessites decreased from 3.96 to 3.75 (see Table 2) as the concentration of Mn^{2+} mixed with the HB0 increased. Though the AOS values of the Zn series birnessites were very similar (see Table 2), the maximum Pb^{2+} adsorption decreased from 3,190 to 2,030 mmol/kg (see Table 3) as the concentration of Zn^{2+} mixed with HB0 increased. The results showed that the maximum Pb^{2+} adsorption capacities of the Mn and Zn series birnessites were significantly less than the HB0 sample, and the maximum Pb^{2+} adsorptions for the Mn series were far less than those of the Zn series samples, for example 1,692 mmol/kg for sample Mn4 vs. 2,290 mmol/kg for sample Zn4 (see Table 3).

The amount of Pb^{2+} adsorbed did not increase with the increase in SSA of birnessites. For the phyllomanganate birnessites, with a high internal surface area, most Pb^{2+} ions are adsorbed on the internal surface. The amount of Pb^{2+} adsorbed was not related directly to the SSA obtained using the method of Brunauer–Emmett–Teller since the SSA could reflect only the external surface of the sample.

Table 1 Mn^{2+} or Zn^{2+} adsorbed on HB0 during treatment

Adsorption of Mn^{2+} or Zn^{2+} to the HB0 at 25±1°C, pH 5.00, and 1.67 g/L birnessite

Mn^{2+} added (mM)	Mn^{2+} adsorbed (mmol/kg)	Zn^{2+} added (mM)	Zn^{2+} adsorbed (mmol/kg)
1	560	1	600
1.5	880	1.5	870
1.8	1,060	1.8	1,060
2	1,170	2	1,170
2.2	1,310	–	–
2.4	1,440	2.4	1,410

Table 2 Mn AOS, SSA, and d (110) values of Mn, Zn series birnessite, and pure HB0

Sample	AOS	SSA (m^2/g)	d(110) (nm)	Sample	AOS	SSA (m^2/g)	d(110) (nm)
HB0	3.96	9.84	0.14160				
Mn1	3.85	27.6	0.14161	Zn1	3.95	63.6	0.14166
Mn2	3.85	39.0	0.14167	Zn2	3.94	49.3	0.14168
Mn3	3.82	44.5	0.14173	Zn3	3.96	40.5	0.14168
Mn4	3.78	50.3	0.14168	Zn4	3.96	37.2	0.14165
Mn5	3.77	56.7	0.14174	–	–		
Mn6	3.75	67.0	0.14196	Zn6	3.96	51.4	0.14169

3.3 Release of Mn^{2+} and Zn^{2+} during the Pb^{2+} adsorption

A part of the pre-adsorbed Mn^{2+} or Zn^{2+} was released from birnessites during Pb^{2+} adsorption (Table 4), while almost no Mn^{2+} was released during Pb^{2+} adsorption on the HB0. The maximum amount of Mn^{2+} released from the Mn series birnessites increased from 86 to 281 mmol/kg (see Table 4) with increasing Mn^{2+} concentrations (see Table 1). No Mn^{2+} was released from the Zn series birnessites, yet the maximum amount of Zn^{2+} released from the Zn series birnessites increased from 155 to 560 mmol/kg (see Table 4) as the concentration of Zn^{2+} increased (see Table 1). In addition, the maximum Mn^{2+} released from the Mn series birnessites was far less than the maximum Zn^{2+} released from the Zn series birnessites, for example 157 mmol/kg for sample Mn4 vs. 312 mmol/kg for sample Zn4 (see Table 4).

4 Discussion

The interaction between Mn^{2+} and birnessite occurs through three possible ways. Firstly, Mn^{2+} ions are adsorbed above or below vacant sites in the structure of birnessite. Secondly, Mn^{2+} ions directly enter and occupy vacant sites. Thirdly, Mn^{2+} ions are oxidized to Mn^{3+} ions which are then adsorbed above or below vacant sites, or Mn^{3+} ions migrate into vacant sites. Lanson et al. (2002b) found that MnO_6 octahedral layers of birnessite with adsorbed heavy metals contained Mn^{3+} and Mn^{4+}, but no Mn^{2+}. Additionally, Silvester et al. (1997) and Drits et al. (1997) showed that if Mn^{3+} in the layer disproportionated into Mn^{2+} and Mn^{4+}, Mn^{2+} is most likely to migrate into the interlayer at pH 5. The results suggest that Mn^{2+} is not stable in the birnessite interlayer. Hence, the second mechanism whereby Mn^{2+} may enter and occupy vacant sites is not possible. During Co^{2+} adsorption on buserite, most Co^{2+} are oxidized to Co^{3+}, which is then adsorbed above or below vacant sites or migrate into vacant sites. The remaining unoxidized Co^{2+} is adsorbed above or below the vacant sites (Manceau et al. 1997). As Mn^{2+} is easily oxidized by birnessite (Tu et al. 1994) and as the radius of Mn^{3+} (0.066 nm) is close to that of Co^{3+} (0.063 nm; Pauling 1960), it is reasonable to suggest that the oxidation of Mn^{2+} to Mn^{3+} on birnessite is similar to the oxidation of Co^{2+} adsorbed on buserite. Therefore, the first and third mechanisms are both possible.

4.1 d(110) interplanar spacing

A large number of vacant sites in a mineral crystal structure will cause distortion of a unit cell parameter (*a*- or *b*-axis) in some lattice plane directions. A large number of vacant sites will also increase the repulsive forces between adjacent cations around the vacant sites, and the coordinating anions of shared octahedra will tend to be drawn closer or pushed farther away (Bailey 1966). For the phyllomanganate birnessite with a high AOS, the increased distortion

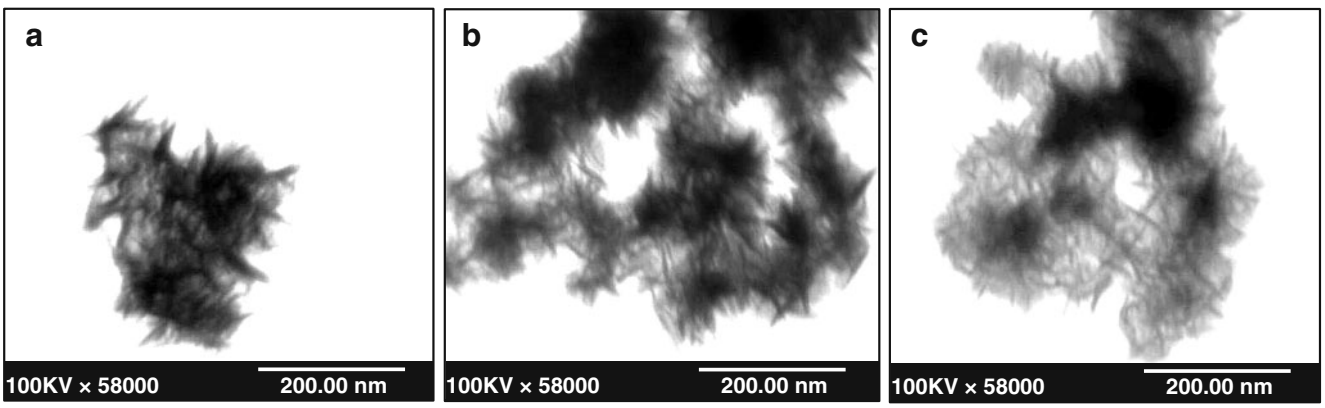

Fig. 2 TEM images of the samples. **a** HB0, **b** Mn6, **c** Zn6

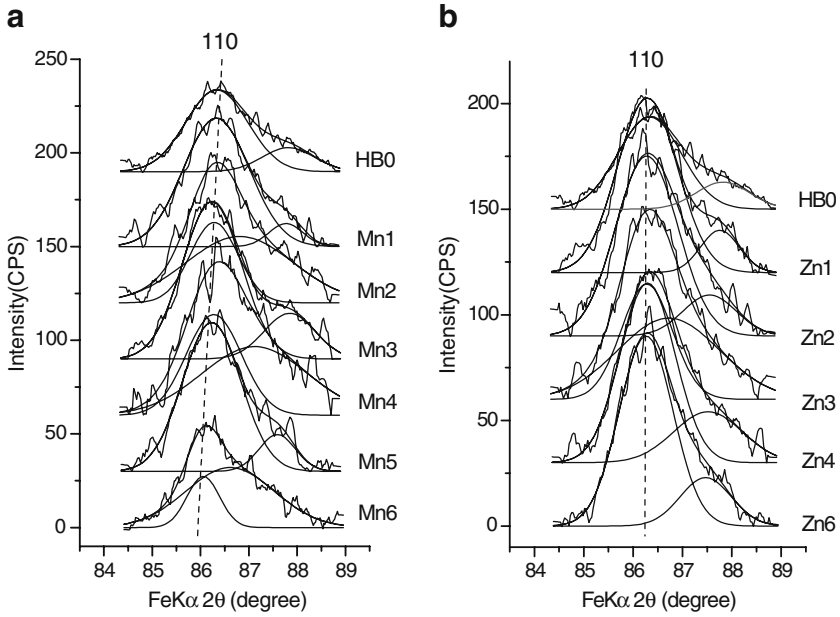

Fig. 3 (110) crystal plane diffraction peaks of samples with two-peak Gaussian fitting. **a** Mn series. **b** Zn series

of the crystal structure along (hk0) will decrease (hk0) interplanar spacings. Hence, changes in (hk0) interplanar spacings (e.g., the 110 reflection) reflect the variation in the number of the vacant Mn octahedral sites (Zhao et al. 2009). For the Zn series birnessites, no significant difference in d(110) interplanar spacing were detected, indicating no detectable change in the number of vacant Mn structural sites. However, for the Mn series birnessites, values of d (110) interplanar spacing increased as AOS decreased (see Table 2), suggesting that the number of vacant Mn structural sites decreased as AOS decreased. Accordingly, oxidation of Mn^{2+} ions to Mn^{3+} by Mn^{4+} at the surface of birnessite results in some of the Mn^{3+} migrating into vacant sites, which decreases the number of vacant sites. The result is similar to the mechanism of Co^{2+} oxidation on buserite (Manceau et al. 1997). As Zn^{2+} ions are adsorbed only above or below vacant sites (Manceau et al. 2002), they will not change the number of vacant sites.

4.2 Mn^{2+} and Zn^{2+} release

The maximum amount of Zn^{2+} released was around twice as much as the maximum amount of Mn^{2+} released during the Pb^{2+} adsorption, suggesting that for the Mn series birnessites, part of the Mn^{3+} derived from the surface oxidation of Mn^{2+} by HB0 migrated into the vacant sites in the structure and was not easily replaced by Pb^{2+}. Mn^{3+} displaced by adsorbed Pb^{2+} would likely disproportionate into Mn^{2+} and Mn^{4+}, with Mn^{4+} ions then migrating into the vacant sites and Mn^{2+} ions being released into solution. Thus,

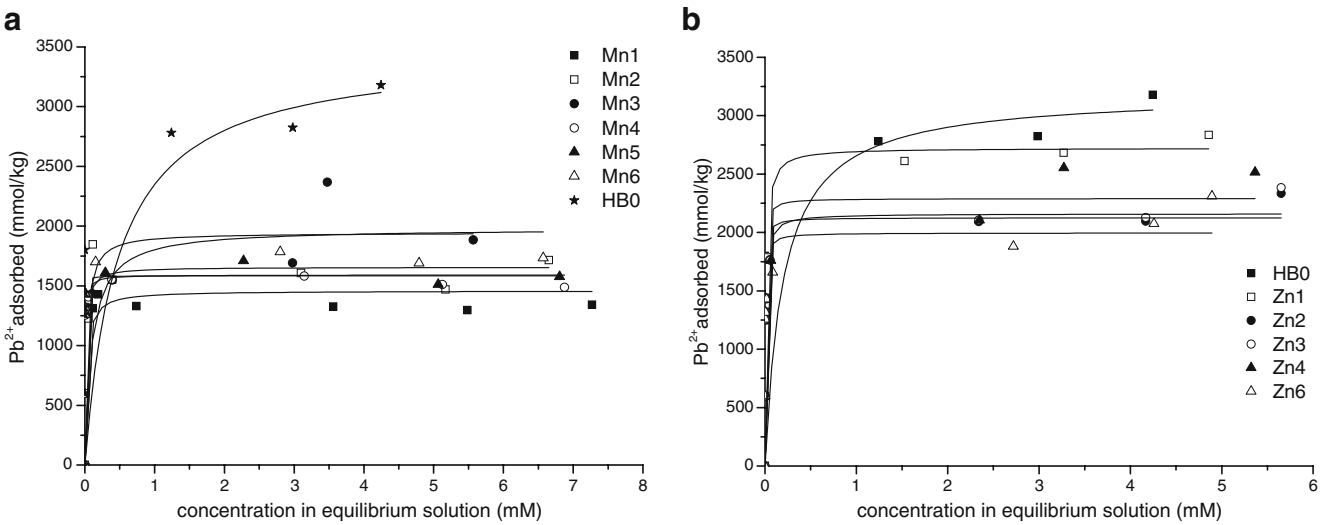

Fig. 4 Isotherms of Pb^{2+} adsorption at 25±1°C, pH 5.00, I=0.1, and 1.67 g/L birnessite. **a** Mn series. **b** Zn series

Table 3 Langmuir parameters for adsorption of Pb^{2+} on the samples

Sample	A_{max} (mmol/kg)	K	r	Sample	A_{max} (mmol/kg)	K	r
HB0	3,190	220.56	0.94				
Mn1	1,785	5,826	0.99	Zn1	2,670	68.86	0.98
Mn2	1,710	1,689	0.96	Zn2	2,160	114.91	0.99
Mn3	1,607	6,656	0.85	Zn3	2110	330.01	0.95
Mn4	1,692	6,750	0.99	Zn4	2,290	265.91	0.96
Mn5	1,581	331	0.99	–	–	–	–
Mn6	1,332	1,355	0.93	Zn6	2,030	348.42	0.96

the concentration of Mn^{2+} ions released from the Mn series birnessites was much less than that of Zn^{2+} ions released from the Zn series birnessites during Pb^{2+} adsorption (see Table 4).

4.3 Hydrolysis constants of the treating Mn^{2+} and Zn^{2+}

The pH used in the study (5.00) is much lower than the hydrolysis constant (pK_1) of Mn^{2+} (pK_{Mn}=10.6) or Zn^{2+} (pK_{Zn}=9.0; Bradbury and Baeyens 2005), indicating that the hydroxylation cations are formed mainly via hydrolysis induced by the surface of birnessite (Weaver et al. 2002; Yu et al. 1996). Hydroxylation of Mn^{2+} or Zn^{2+} lowered the energy barriers for specific adsorption and thus enhanced adsorption. Such an effect is more significant for heavy metals with greater hydrolysis constants. The first-order hydrolysis constant of Zn^{2+} is larger than that of Mn^{2+}, indicating that the competitive effect of Zn^{2+} on Pb^{2+} adsorption is stronger than Mn^{2+}. The sequence of maximum Pb^{2+} adsorption of Zn series birnessites > Mn series birnessites (see Table 3) indicates that the mechanism of Mn^{2+} interacting with birnessite is different from that of Zn^{2+}. When the HB0 was treated with Mn^{2+}, part of the Mn^{3+}, derived by the oxidation of Mn^{2+}, likely migrated into vacant sites in the structure, decreasing the Pb^{2+} adsorption capacity.

4.4 Maximum Pb^{2+} adsorption

The maximum amounts of Pb^{2+} adsorbed on the Zn series birnessites (2,030–2,670 mmol/kg) were generally greater than the maximum Pb^{2+} adsorbed on the Mn series birnessites (1,330–1,740 mmol/kg, see Table 3). The sum of maximum Pb^{2+} adsorbed for the Zn series birnessites and residual Zn^{2+}, which is the difference between the amount of Zn^{2+} released during Pb^{2+} adsorption and the amount of Zn^{2+} added initially, is close to the total Pb^{2+} adsorption capacity of HB0 (Table 5).

Specific adsorption sites for Zn^{2+} or Pb^{2+} on birnessite are located mainly above or below vacant sites, indicative of a competitive relationship between Zn^{2+} and Pb^{2+} for the vacant sites (Lanson et al. 2002b). The number of vacant sites remained unchanged in the structure of the Zn series birnessites in comparison with HB0 (based on values of spacings for the 110 reflection), indicating that the number of adsorption sites remained the same. Consequently, the sum of maximum Pb^{2+} adsorption and residual Zn^{2+} in the Zn series birnessites is close to the Pb^{2+} adsorption capacity of HB0.

Since the radius of Pb^{2+} (0.120 nm) is much larger than that of Mn^{3+} (0.066 nm) and Mn^{4+} (0.054 nm; Pauling 1960), it is impossible for Pb^{2+} to displace structural Mn^{3+} or Mn^{4+} in MnO_6 octahedral layers. Therefore, Mn^{2+} released during Pb^{2+} adsorption is derived mostly from interlayer Mn^{2+} or Mn^{3+} located above or below the vacant Mn octahedral sites (Matocha et al. 2001). For the Mn series birnessites, 11.4–20.6% of the pre-adsorbed Mn^{2+} was released during Pb^{2+} adsorption, suggesting that part of the Mn^{2+} pre-adsorbed, either as of Mn^{2+} or Mn^{3+}, should be located above or below the vacant sites in birnessite. Firstly, it is assumed that residual Mn^{2+}, in samples with adsorbed Pb^{2+}, is located above or below vacant sites, similar to the location of Zn^{2+}. For the Mn series birnessite, the sum of the maximum Pb^{2+} adsorption and residual Mn^{2+}, which is the difference between the amount of Mn^{2+} released during Pb^{2+} adsorption and the amount of Mn^{2+} added, should be close to the Pb^{2+} adsorption capacity of HB0. However,

Table 4 Maximum amounts of Mn^{2+} and Zn^{2+} released during the Pb adsorption (mmol/kg)

Sample	Maximum Mn^{2+} release	Sample	Maximum Zn^{2+} release
HB0	7		
Mn1	86	Zn1	155
Mn2	100	Zn2	249
Mn3	172	Zn3	285
Mn4	157	Zn4	312
Mn5	270	–	–
Mn6	281	Zn6	560

Table 5 Maximum Pb^{2+} adsorption and maximum Zn^{2+} released during the Pb^{2+} adsorption (mmol/kg)

Sample	Zn^{2+} added	Pb^{2+} adsorbed	Zn^{2+} released	Zn^{2+} residual	(Zn^{2+} residual+Pb^{2+} adsorbed)
HB0	0.00	3,190	0.00	0.00	3,190
Zn1	600	2,670	155	445	3,115
Zn2	870	2,160	249	621	2,781
Zn3	1,060	2,110	285	775	2,885
Zn4	1,170	2,290	312	858	3,148
Zn6	1,410	2,030	560	850	2,880

sums (2,214–2,623 mmol/kg) were much less than the Pb^{2+} adsorption capacity of HB0 (3,190 mmol/kg, Table 6), indicating that this assumption is not correct. Secondly, it was assumed that residual Mn ions located in the layer were present as Mn^{3+}. According to the literature, the proportion of vacant sites in the birnessite structure does not exceed 16.7% of the Mn content (Manceau et al. 2002). In addition, based on the results of Feng et al. (2007), birnessite molecular weight can be assumed as 100 g/mol. If Pb^{2+} ions adsorbed are located only above or below the vacant sites, the maximum Pb^{2+} adsorption of birnessite will not exceed 1,670 mmol/kg. The much larger Pb^{2+} adsorption capacity of HB0 (3,190 vs. 1,670 mmol/kg) suggests that Pb^{2+} adsorption occurs both above and below vacant sites in HB0. Therefore, each Mn^{3+} ion occupying a vacant site could be considered as occupying two adsorption sites. Occupation of vacant sites by Mn^{3+} effectively reduces the number of adsorption sites for Pb^{2+}. Hence, the adsorption capacity of HB0 decreases. The sum of maximum Pb^{2+} adsorption of Mn series birnessites and the twice residual Mn^{2+} (in form of Mn^{3+}) should be close to the Pb^{2+} adsorption capacity of HB0 (see Table 6). However, the sums (2,688–3,648 mmol/kg) are generally more than the Pb^{2+} adsorption capacity of HB0 (3,190 mmol/kg) except for 2,688 mmol/kg for Mn1, indicating that not all residual Mn^{2+} ions are located in the layer. Therefore, except for a small part of unoxidized Mn^{2+} located above or below the vacant sites, most Mn^{2+} was oxidized to Mn^{3+} by HB0. A portion of the Mn^{3+} produced, located above or below the vacant sites, did not affect the number of vacant sites, and the remaining Mn^{3+} may have migrated into and filled up the vacant sites. Occupation of vacant sites will significantly decrease the maximum Pb^{2+} adsorption in comparison with HB0. Consequently, considering our previous results (Zhao et al. 2009), the Pb^{2+} adsorption capacity of birnessites is mainly determined by the number of vacant Mn sites they possess.

5 Conclusions

The number of vacant Mn octahedral sites in Zn^{2+}-treated birnessites remained almost unchanged as the nominal concentration of Zn^{2+} increased. The maximum Pb^{2+} adsorption capacity of birnessite decreased due to Zn^{2+} occupying adsorption sites. The AOS of Mn^{2+}-treated birnessites decreased and most of the Mn^{2+} ions added were oxidized to Mn^{3+} ions. The number of vacant Mn octahedral sites in the Mn^{2+}-treated birnessites decreased due mainly to the presence of Mn^{3+} migrated into vacant Mn octahedral sites. Moreover, the maximum Pb^{2+} adsorption of Zn^{2+}-treated birnessite was greater than for the Mn^{2+}-treated birnessite. These results indicate that the Pb^{2+} adsorption capacity of birnessite is largely determined by the number of Mn site vacancies.

6 Recommendations and perspectives

Adsorption is one of the important processes that affect the transfer of heavy metals, such as Pb from the aqueous

Table 6 Maximum Pb^{2+} adsorption and maximum Mn^{2+} released during the Pb^{2+} adsorption (mmol/kg)

Sample	Mn^{2+} added	Pb^{2+} adsorbed	Mn^{2+} released	Mn^{2+} residual	(Mn^{2+} residual+Pb^{2+} adsorbed)	($2Mn^{2+}$ residual+Pb^{2+} adsorbed)
HB0	0	3,190	7	0	3,190	3,190
Mn1	560	1,740	86	474	2,214	2,688
Mn2	880	1,630	100	780	2,410	3,190
Mn3	1,060	1,450	172	888	2,338	3,226
Mn4	1,170	1,610	157	1,013	2,623	3,636
Mn5	1,310	1,550	270	1,040	2,590	3,630
Mn6	1,440	1,330	281	1,159	2,489	3,648

to the solid phase, thus influencing their distribution, mobility, and bioavailability. As the most common Mn oxide in soils, birnessites possess the greatest adsorption affinity and capacity for Pb^{2+} among heavy metal ions. Further studies of the structure of birnessite and the reactivity of birnessite with Pb are essential to predict the fate and transport of Pb in the environments and to optimize remediation measures.

Acknowledgments We thank Professor Cai Xian Tang at La Trobe University, Australia for reviewing the final draft. The supports of the National Natural Science Foundation of China (no. 40771102), the Foundation for the Author of National Excellent Doctoral Dissertation of PR China (no. 200767), and the Natural Science Foundation for Distinguished Young Scholars of Hubei Province (no. 2007ABB014) are acknowledged.

References

Ahn M-Y, Filley TR, Jafvert CT, Nies L, Hua I (2006) Birnessite mediated debromination of decabromodiphenyl ether. Chemosphere 64:1801–1807

Appelo CAJ, Postma D (1999) A consistent model for surface complexation on birnessite (-MnO2) and its application to a column experiment. Geochim Cosmochim Acta 63:3039–3048

Bailey SW (1966) The status of clay mineral structures. Clay Clay Miner 14:1–23

Bradbury MH, Baeyens B (2005) Modelling the sorption of Mn(II), Co (II), Ni(II), Zn(II), Cd(II), Eu(III), Am(III), Sn(IV), Th(IV), Np(V) and U(VI) on montmorillonite: linear free energy relationships and estimates of surface binding constants for some selected heavy metals and actinides. Geochim Cosmochim Acta 69:875–892

Burns RG (1976) The uptake of cobalt into ferromanganese nodules, soils, and synthetic manganese(IV) oxides. Geochim Cosmochim Acta 40:95–102

Chang Chien SW, Chen HL, Wang MC, Seshaiah K (2009) Oxidative degradation and associated mineralization of catechol, hydroquinone and resorcinol catalyzed by birnessite. Chemosphere 74:1125–1133

Drits VA, Silvester E, Gorshkov AI, Manceau A (1997) Structure of synthetic monoclinic Na-rich birnessite and hexagonal birnessite. I. Results from X-ray diffraction and selected-area electron diffraction. Am Mineral 82:946–961

Feng XH, Zhai LM, Tan WF, Liu F, He JZ (2007) Adsorption and redox reactions of heavy metals on synthesized Mn oxide minerals. Environ Pollut 147:366–373

Giles CH, MacEwan TH, Nakhwa SN, Smith D (1960) Studies in adsorption, Part XI. A system of classification of solution adsorption isotherms and its use in diagnosis of adsorption mechanisms and in measurement of specific surface area of solids. J Chem Soc 3:3973–3993

Golden DC, Chen CC, Dixon JB (1987) Transformation of birnessite to buserite, todorokite, and manganite under mild hydrothermal treatment. Clay Clay Miner 35:271–280

Kijima N, Yasuda H, Sato T, Yoshimura Y (2001) Preparation and characterization of open tunnel oxide [alpha]-MnO_2 precipitated by ozone oxidation. J Solid State Chem 159:94–102

Kinniburgh DG (1986) General purpose adsorption isotherms. Environ Sci Technol 20:895–904

Lanson B, Drits VA, Feng Q, Manceau A (2002a) Structure of synthetic Na-birnessite: evidence for a triclinic one-layer unit cell. Am Mineral 87:1662–1671

Lanson B, Drits VA, Gaillot A-C, Silvester E, Plancon A, Manceau A (2002b) Structure of heavy-metal sorbed birnessite: Part 1. Results from X-ray diffraction. Am Mineral 87:1631–1645

Manceau A, Charlet L (1992) X-ray absorption spectroscopic study of the sorption of Cr(III) at the oxide–water interface: I. Molecular mechanism of Cr(III) oxidation on Mn oxides. J Colloid Interf Sci 148:425–442

Manceau A, Drits VA, Silvester E, Bartoli C, Lanson B (1997) Structural mechanism of Co(super 2+) oxidation by the phyllomanganate buserite. Am Mineral 82:1150–1175

Manceau A, Lanson B, Drits VA (2002) Structure of heavy metal sorbed birnessite. Part III: results from powder and polarized extended X-ray absorption fine structure spectroscopy. Geochim Cosmochim Acta 66:2639–2663

Matocha CJ, Elzinga EJ, Sparks DL (2001) Reactivity of Pb(II) at the Mn(III, IV) (oxyhydr)oxide–water interface. Environ Sci Technol 35:2967–2972

McKenzie RM (1971) The synthesis of birnessite, cryptomelane, and some other oxides and hydroxides of manganese. Miner Mag 38:493–503

McKenzie RM (1980) The adsorption of lead and other heavy metals on oxides of manganese and iron. Aus J Soil Res 18:61–73

O'Reilly SE, Hochella MF (2003) Lead sorption efficiencies of natural and synthetic Mn and Fe-oxides. Geochim Cosmochim Ac 67:4471–4487

Pauling L (1960) The nature of the chemical bond and the structure of molecules and crystals: an introduction to modern structural chemistry, 3rd edn. Cornell University Press, New York

Peacock CL, Sherman DM (2007) Sorption of Ni by birnessite: Equilibrium controls on Ni in seawater. Chem Geol 238:94–106

Post JE (1999) Manganese oxide minerals: crystal structures and economic and environmental significance. PNAS 96:3447–3454

Silvester E, Manceau A, Drits VA (1997) Structure of synthetic monoclinic Na-rich birnessite and hexagonal birnessite. II. Results from chemical studies and EXAFS spectroscopy. Am Mineral 82:962–978

Toner B, Manceau A, Webb SM, Sposito G (2006) Zinc sorption by biogenic hexagonal birnessite particles within a hydrated biofilm. Geochim Cosmochim Ac 70:27–43

Tu S, Racz GJ, Goh TB (1994) Transformations of synthetic birnessite as affected by pH and manganese concentration. Clay Clay Miner 42:321–330

Villalobos M, Toner B, Bargar J, Sposito G (2003) Characterization of the manganese oxide produced by *pseudomonas putida* strain MnB1. Geochim Cosmochim Acta 67:2649–2662

Villalobos M, Bargar J, Sposito G (2005) Mechanisms of Pb(II) sorption on a biogenic manganese oxide. Environ Sci Technol 39:569–576

Villalobos M, Lanson B, Manceau A, Toner B, Sposito G (2006) Structural model for the biogenic Mn oxide produced by *Pseudomonas putida*. Am Mineral 91:489–502

Weaver RM, Hochela MF, Ilton ES (2002) Dynamic processes occurring at the CrIIIaq-manganite (γ-MnOOH) interface: Simultaneous adsorption, microprecipitation, oxidation/reduction, and dissolution. Geochim Cosmochim Ac 66:4119–4132

Webb SM, Tebo BM, Bargar JR (2005) Structural characterization of biogenic Mn oxides produced in seawater by the marine *Bacillus* sp. strain SG-1. Am Mineral 90:1342–1357

Xu Y, Boonfueng T, Axe L, Maeng S, Tyson T (2006) Surface complexation of Pb(II) on amorphous iron oxide and manganese oxide: spectroscopic and time studies. J Colloid Interf Sci 299:28–40

Yu TR, Ji GL, Ding CP (1996) Electrochemistry of variable charge soils. Science Press, Beijing, pp 67–87

Zhao W, Cui HJ, Feng XH, Tan WF, Liu F (2009) Relationship between Pb2+ adsorption and average Mn oxidation state in synthetic birnessites. Clay Clay Miner 57:338–345